Experimental study of thick composites stability under thermal loading using 3D ESPI set-up

Jérôme Molimard, Andrés Dolinko, Guillermo H Kaufmann

Experimental study of thick composites stability under thermal loading using 3D ESPI set-up

J. Molimard[a], A. E. Dolinko[b] and G. H. Kaufmann[c]

Abstract

Due to the impulsion of aircraft manufacturers, Carbon Fibre Reinforced Polymers have become thicker. But the manufacturing process still implies the development of important residual stresses, either due to moisture effects or thermal effects [1]. If the symmetry of the composite part is broken, the global part shape will be affected by any moisture/temperature variation. In this communication, a simple L thick composite shell is studied under moderate temperature changes. An error in the stacking sequence is voluntarily added to the sequence in order to simulate possible manufacturing error. Displacements are recorded on the shell front and on its side using a mixed in-plane and out-of-plane DSPI set-up [8]. The zone of interest is limited here to the central part of the L shape i.e. where the curvature is significant. Variations of the L-shape with temperature are recorded; typical flexure strain effects are outlined. Interesting global or local parameters can be deduced from this experiment: through thickness coefficient of thermal expansion, ply thickness and consequently local fibre volume fraction.

Keyword optical technique: *DSPI, fringe projection, digital image correlation*

Keyword application: *airplane structural analysis*

---

contact information

[a] molimard@emse.fr
SMS/LTDS, UMR CNRS 5513, Ecole des Mines de Saint-Etienne,
158 cours Fauriel, 42023 Saint-Etienne cedex 02, France
[b] dolinko@ifir-conicet.gov.ar
Instituto de Física Rosario (CONICET-UNR),
Bvd. 27 de Febrero 210 bis, S2000EZP Rosario, Argentina
[c] kaufmann@ifir-conicet.gov.ar
Instituto de Física Rosario (CONICET-UNR),
Bvd. 27 de Febrero 210 bis, S2000EZP Rosario, Argentina

Introduction

Composite laminates for structural applications are commonly processed under high temperature compared to their working conditions (180 °C vs. 25 °C). Coefficients of thermal expansion mismatch combined with different stiffness from one component to the other imply the development of high internal stresses [1]. These stresses can even cause the structure's failure without any external loading (micro-cracking of transverse ply). Another consequence of these internal stresses is a lack of dimensional stability, especially in the case of non symmetric parts, but such effect can occur even if the stacking sequence is symmetric. Theoretically, such a situation is not predictable if the components volume fraction is nominal. In fact, the shape variation sources have to be found in the defaults induced by the manufacturing process, especially the variations in the components distribution.

We propose here an experimental study on a typical L shape submitted to a temperature change; the stacking sequence is symmetric, but we simulate an error in the manufacturing process by adding an extra ply to the sequence. Chosen composite coupon is rather thick (9.5 mm) to simulate realistic industrial application.

Strain fields have to be recorded first on the coupon side, second on its face. Due to the particular shape of the specimen, expected displacement fields are both in plane (x and y axis) and out of plane (z axis); the difficulty here is to define the appropriate plane in the analysis, the specimen being non-planar. Expected displacements are supposed to be small; finally, the chosen optical full-field technique is a 3D ESPI set-up for displacement measurements coupled with fringe projection set-up for shape measurement. This approach is simpler than the one proposed by Goudemand [2]. Here, the fringes are projected by a classical video-projector and not by the DSPI sources.

Shape measurement using fringe projection technique

The fringe projection method [1][3] has been selected as a reasonable tool for measuring the specimen shape. The physical principle of the fringe projection method is straightforward: A periodic pattern of white and black lines is projected on an object; the light is diffused by the object and captured by a CCD video-camera (Figure 1). The deformation of the fringes, recorded as phase maps, has a known dependency to the out-of-plane contour variations of the illuminated object.

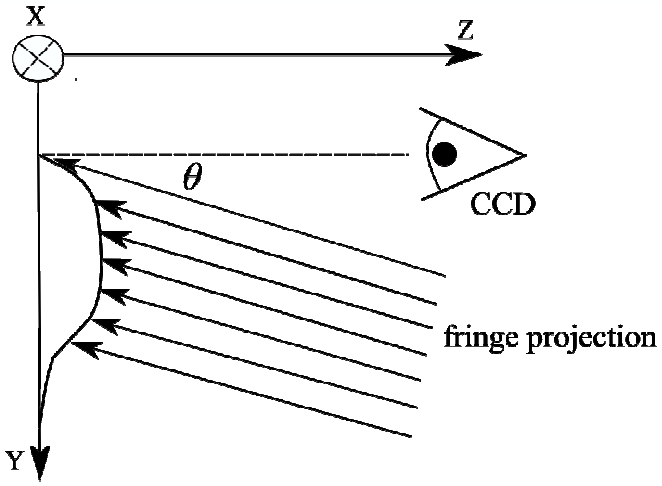

Figure 1: *Fringe projection basic principle.*

The fringe projection technique exploits the light diffused by an object in order to measure its shape or shape variation. Moreover, in order to observe out-of-plane displacements, the angle between the projected fringes and the observed diffused light must not be null. Light intensities on an object illuminated by a set of fringes can be described by a periodic function I_{li}, with a perturbation ϕ corresponding to the object shape:

$$I_{li}(x,y) = I_0(x,y)\left[1+\gamma(x,y)\cos\left(\frac{2\pi}{p(x,y)}y+\varphi^{FP}(x,y)\right)\right] \quad (1)$$

This equation involves an average intensity I_0 and a contrast γ. These values should be constant over the whole map, but some low-frequency variations due to illumination inhomogeneities or diffusivity changes on top of the surface can occur. Consequently, both average intensity and contrast have to be considered as local quantities, typically calculated over few fringe periods, and can be denoted $I_0(x,y)$ and $\gamma(x,y)$. The pitch p is the distance between two light peaks on a flat surface. Again, due to perspective effects in particular, this pitch can change over the map, but this variation can be known either using a model or a calibration procedure.

Lastly, the object is responsible for a phase shift $\phi^{FP} = \phi^{FP}(x,y)$ at each point of the field. Consequently, eqn (1) is based on three unknown quantities ($I_0(x,y)$, $\gamma(x,y)$,$\phi(x,y)$) which need at least three equations to be identified. The phase is extracted through the home-made code Photomecanix and the out-of-plane position $Z(x,y)$ can be retrieved from to the following basic equation:

$$\varphi^{FP}(x,y) = \frac{2\pi\tan(\theta(x,y))}{p(x,y)}Z(x,y) \quad (2)$$

In this expression, the sensitivity characterized by the slope of the linear relationship between $\phi^{FP}(x,y)$ and $Z(x,y)$, can be adjusted by modifying the pitch p or the angle θ between the CCD video-camera and the video-projector. It has to be noted that the sensitivity can vary locally. In particular, in the present experiment, the video projector and the CCD camera used divergent beams, leading to a more complex situation than the one described in Figure 1. A specific calibration procedure has been developed based on prescribing a known translation of a reference object. The phase variation ϕ^{FP} is extracted using a temporal phase shifting algorithm proposed by Surrel [4]; the phase shifter is the video-projector itself, controlled by Photomecanix. Last, no camera distortion model has been applied here.

An estimation of the resolution based on a repeatability test on a given stable situation gives a value of 0.9 % of one fringe, i.e. the noise level is 20 µm. Because of the use of the temporal phase shifting algorithm, spatial resolution is kept to 1 pixel i.e. from 18.6 to 29.3 µm depending on the experiment.

Displacements measurement using DSPI set-up

To measure the $u(x,y)$ $v(x,y)$ and $w(x,y)$ components of the displacement field at the surface of an object, three speckle interferometers with in-plane and out-of-plane sensitivity are used.

The basic equation of DSPI that describes the optical phase difference $\Delta\phi$ due to the displacement u of the object is given by

$$\Delta\varphi^{DSPI}(x,y) = 2\frac{\pi}{\lambda}(e_i - e_o)\cdot u \tag{3}$$

where $\boldsymbol{e_i}$ and $\boldsymbol{e_o}$ are the illumination and the observing unit vectors, respectively, and λ is the wavelength of the laser light.

Here the specimen is observed along $\boldsymbol{e_o}$=(0,0,-1) and is illuminated with three different beams, using the same reference beam as for a classical out-of-plane set-up. Two beams are in an horizontal plane, i.e. $\boldsymbol{e_1}$=(sin γ_1, 0, cos γ_1) and $\boldsymbol{e_2}$=(sin γ_2, 0, cos γ_2), $\gamma_2 \approx -\gamma_1$, while the last one is in a vertical plane, i.e. $\boldsymbol{e_3}$=(0, sin γ_3, cos γ_3). The phase changes between both object beams and the reference are given by:

$$\begin{Bmatrix} \Delta\varphi_1^{DSPI}(x,y) \\ \Delta\varphi_2^{DSPI}(x,y) \\ \Delta\varphi_3^{DSPI}(x,y) \end{Bmatrix} = \frac{2\pi}{\lambda}\begin{bmatrix} \sin\gamma_1 & 0 & (1+\cos\gamma_1) \\ \sin\gamma_2 & 0 & (1+\cos\gamma_2) \\ 0 & \sin\gamma_3 & (1+\cos\gamma_3) \end{bmatrix}\begin{Bmatrix} u_1(x,y) \\ u_2(x,y) \\ u_3(x,y) \end{Bmatrix} \tag{4}$$

where Δu_1, Δu_2 and Δu_3 are respectively the in-plane and out-of-plane displacement components. In fact, due to the specimen geometry and the lens divergence, γ_i, i=1..3 is not constant over the covered field. Knowing the optical arrangement and the specimen geometry, it is possible to determine pointwisely $\gamma_i(x,y)$. As a general form, each sensitivity vector ($\boldsymbol{e_i}$-$\boldsymbol{e_0}$) is expressed according to the optical centres of the divergent beam and the camera, and the local position of each surface point M. The frame of reference is shown in Figure 2 (red arrows). For each couple illumination beam / reference beam, the phase is extracted throw a temporal phase shifting algorithm, and, if necessary, and unwrapping algorithm described in [5].

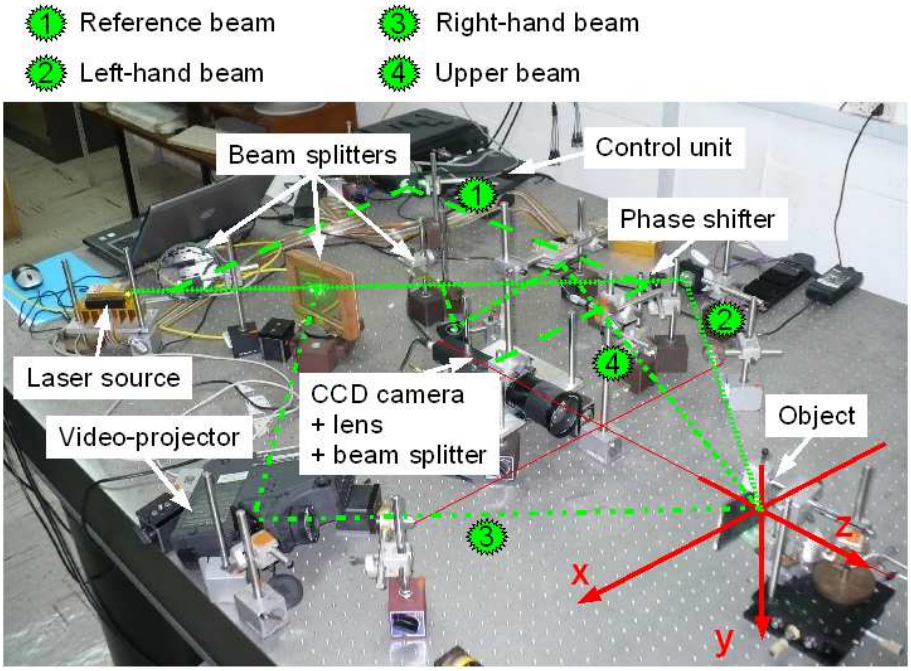

Figure 2: *Optical arrangement*

Experiments

experimental set-up

The DSPI system used to measure the displacement field is shown in Figure 2. The light from a doubled-YAG laser with a wavelength λ=532 nm is divided by a tunable beam-splitter into a reference beam (denoted 1) and 3 beams illuminating the object (denoted 2~4). Each of these latter beams are separated using tunable beam splitters. Both beams are expanded by microscope objectives, illuminate the specimen and the diffused light interferes with the reference beam. The specklegram is imaged by a CCD camera (Pulnix TM-620) whose output is fed to a frame grabber (Matrox Pulsar) located inside of a personal computer which digitises images with a resolution of 512 x 512 pixels x 8 bits. The video camera has a zoom lens which allows to image a small region of the specimen of about 18 mm x 18 mm. A piezoelectric transducer linked to one of the mirrors (M) is used to perform the phase shifting. This transducer is linearly displaced by the control unit. A video-projector ensures the fringe projection with an mean angle of incidence close to 30°.

Uncertainty analysis

In the following experiments, the camera centre is located at point {0, 0, - 450}' mm, and the illumination beams foci respectively at {-505, 0, - 450}' mm, {0, -229, -450}' mm, {485, 0, - 450}' mm.

These values are one order of magnitude higher than the region of interest size (18 × 18 mm^2). In fact, if the surface is flat, i.e. that each measuring point is in the plane / M(x, y, 0) $\forall$ x, y , the beam divergence has few influence on the result. Figure 3 shows typical error maps for a representative loading condition, in this case a temperature change of 9°C. Under these experimental conditions, the error without using the beam divergence is lower than 2 %.

Points with different positions should also lead to some uncertainties. In order to evaluate the error on these positions, a variation on the vertical illumination focus has been imposed ; because the position is measured using a rule with precision of 1 mm on its two ends, the variation has been set to +1.4 mm on each direction. Then, the maximum error encountered on the experimental map is 1 % (see figure 4).

Last, on flat surfaces, errors related to the surface position are mainly due to the vertical axis: the two others being symmetric, a simple reflective surface is sufficient to minimize any left/right misalignment. We can suppose that on a 18 × 18 mm^2 surface, a variation of ±1 mm is reasonable on the vertical direction. The relative error related to this event gives a maximum value of 0.18 %.

If extending these results using classical error propagation rules [6], the overall error on elements position is lower than 2 % (using the divergence beam formulation) or lower than 2.7 % if the divergence effect is neglected. Finally, the variations on displacements induce few effects on strain maps. Induced errors are lower than 2 µm/m ; this can be explained by the pixels size, and consequently the derivation kernel, and by the low-frequency shape of error functions.

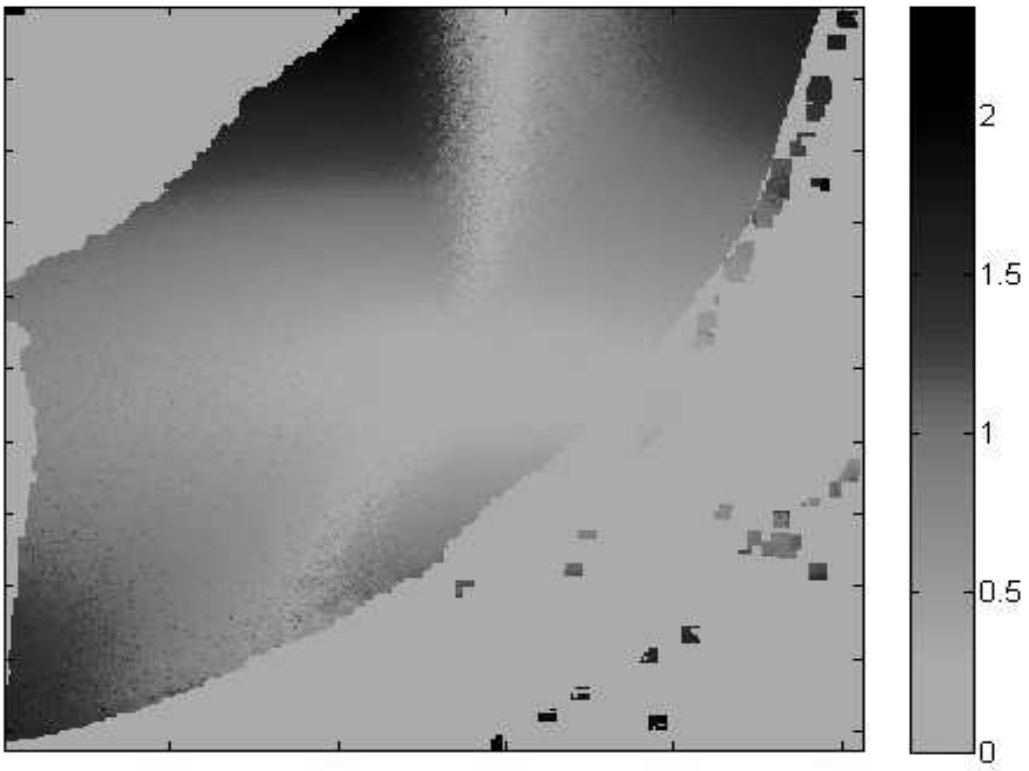

Figure 3: *Relative error on the displacement norm if not considering the divergence (for a specimen submitted to a 9°C temperature change, viewed from its flat side)*

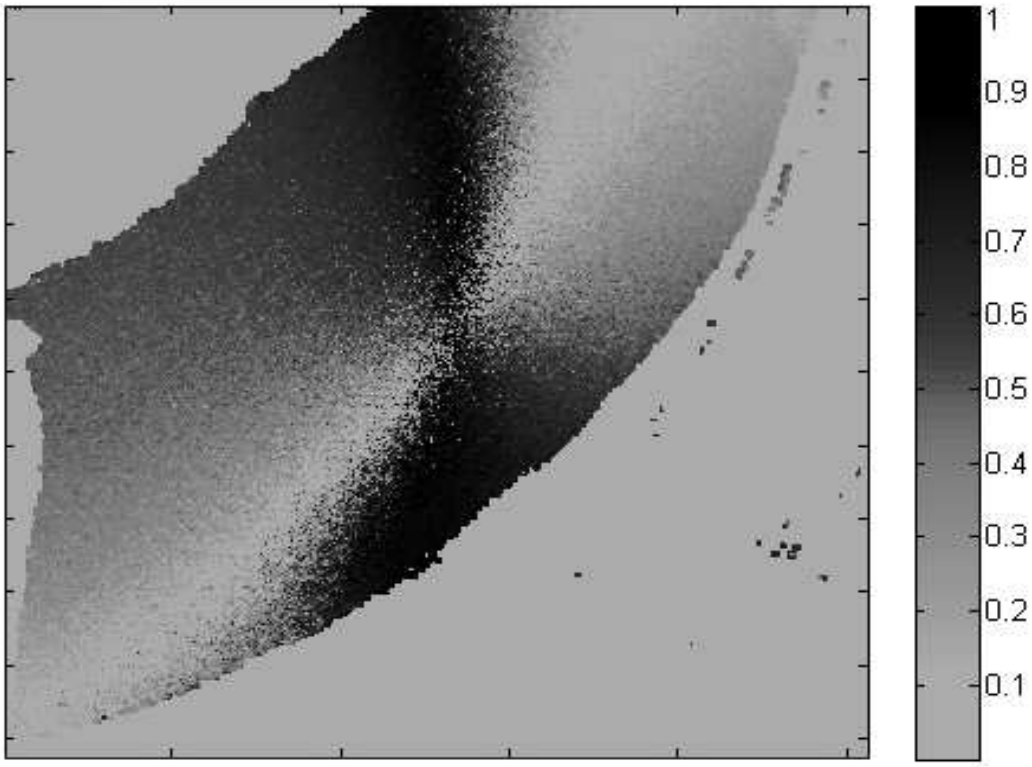

Figure 4: *Relative error on the displacement norm due to uncertainties on illumination beam position (for a specimen subjected to a 9°C temperature change, viewed from its flat side)*

Temperature set-up

Expected temperature changes are below 35 °C. These small changes were selected due to the very high sensitivity of DSPI, and because of the versatility of heating systems in such a range. Here, an halogen lamp has been placed beside the specimen. A screen avoids light to propagate in the direction of the camera in such a form that no noise is added to the signal.

Experimental conditions have been optimized to generate an homogeneous temperature field over the area of interest. In fact, temperature variations over the field are lower than 1 °C, and from de back side to the front side of the specimen lower than 2°C. Lastly, a repeatability test shows that the temperature resolution is 1.5 °C.

Results and analysis

Specimen

The specimen used for this experiment is a $[0\ 90]_{60}$ laminate of Carbon Fibre Reinforced Polymer T300 from Hexcel Company. It should be noticed that the sample is slightly non-symmetric: an extra 0 (or 90) ply is added to simulate a possible error during the manufacturing process. It is cured in a rigid mould. Its final geometry is an L-shape. The L inner and outer curvature radii are respectively 9 mm and 21 mm. the total mean thickness is 9.5 mm [7].

Results will be presented here for a temperature change of 12.4 K. A set of 3D displacement fields is recorded both from the front side and from the left side of the specimen, as described in figure 5. The total covered area is 18×18 mm^2. For clarity of the purpose, only results on the left side will be presented here.

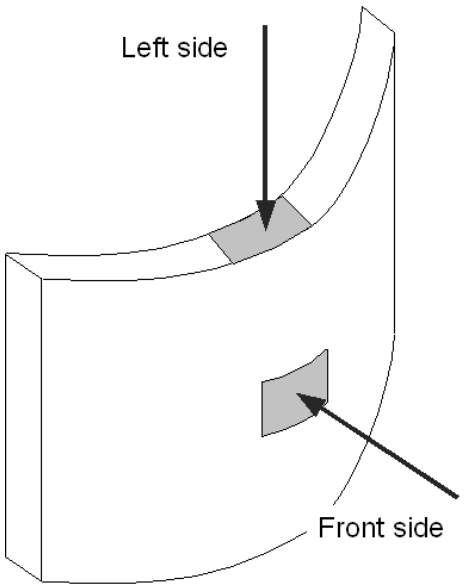

Figure 5: *Schematic view of the specimen and measuring areas*

Results

Left side results should have been taken with two classical in-plane ESPI interferometers. In fact, we used here a 3D set-up, adding extra information (out-of-plane). Displacements found in x- and y- directions follow the specimen curvature (Figure 6). Because it is a quasi-plane

situation, the strain has been calculated in this case. In spite of the natural curvature, the average orientation of the specimen is 45° off the horizontal axis. The specimen mainly expands throughout its thickness. This result is commonly found for composite materials, where the fibres have a lower dilatation coefficient than the resin. If the strain are projected in a specimen frame of reference, ε_{xx} and ε_{yy} are constant, with respective mean values of 136 10^{-6} and 529 10^{-6}. Consequently, it is possible to estimate the coefficient of thermal expansion of 11.3 10^{-6} m/m/K, and a throw thickness coefficient of 58.0 10^{-6} m/m/K. Even if the order of magnitude is in agreement with common knowledge, a fine comparison is difficult, mainly because the fibre volume fraction varies within the curvature area. The specimen is subjected to an almost constant shear and a progressive rotation in the Earth frame of reference. Again, using the specimen coordinate system, shear is different, and it varies linearly with the actual position along the sample. Therefore, using a beam approximation, this implies that the bending moment varies quadratically with the position.

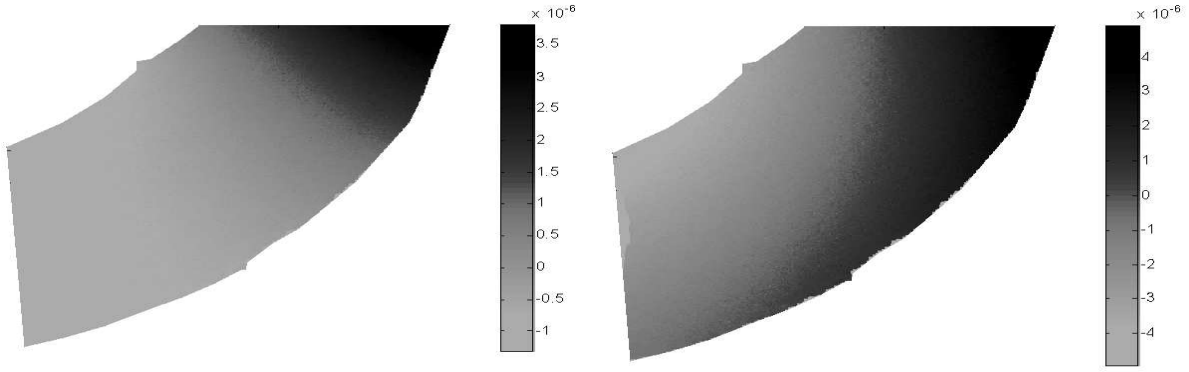

Figure 6: *Left side – x- and y-displacements for a temperature change of 12 K (in m).*

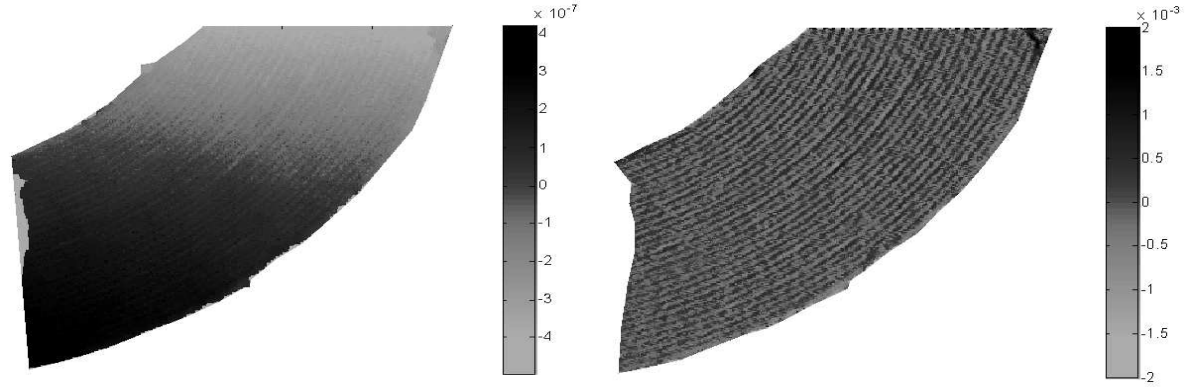

Figure 7: *Left side – z-displacement field, and displacement gradient. The plies of the part are clearly outlined.*

Finally, the out-of plane displacement field has been also recorded and analysed. Of course, the order of magnitude of the displacement is much smaller than the two others. It is believed that the main source of out-of-plane displacement is related to the boundary effects, and clamping variations with temperature because no low-frequency gradient is visible. Now, high frequency information, corresponding to the plies stacking sequence, is visible (Figure 7). These plies behave in a different way from one to the other because of their different

dilatation coefficient in this direction, due to fibres orientation. Analysing the signature leads to a mean ply thickness of 183.5 µm. The nominal ply thickness is 152 µm, so that, it is possible to estimate the effective fibre volume fraction: 49% instead of 59%.

The local effect also shows the very good spatial resolution achieved with this DSPI set-up: each ply has a mean measured thickness of 9.9 pixels, and the spatial resolution using the autocorrelation function on noise gave a value of 1 pixel.

Conclusion

The geometrical variations of a thick L-shape composite coupon subject to a temperature change have been recorded by a 3D DSPI set-up. The system takes into account the local variations of the three sensitivity vectors related to the beam divergence and to the specimen shape variations. Errors uncertainties due to the calibration procedure are supposed to be lower than 2 % for the displacements and 2µm/m for the strains, strains being calculated performing a low-pass filtering and derivation over 11 pixels.

First results on the composite sample show that: 1st, the composite shape changes as if the part where subjected to a quadratic bending moment. 2nd, thermal expansion coefficients could be identified in-situ, with realistic values. 3rd, the ply thickness, and consequently the fibre volume fractions were found to be lower than the nominal value (49% instead of 59%.).

Further work will concern the projection of strains in the local co-ordinate system, and the analysis of the front side results.

References

[1] GIGLIOTTI, M., JACQUEMIN, F., MOLIMARD, J., VAUTRIN, A., Transient and cyclical hygrothermoelastic stress in laminated composite plates: Modelling and experimental assessment, Mechanics of Materials, 39 (8): 729-745, 2007.

[2] N. GOUDEMAND, 3D-3C Speckle interferometry: optical device for measuring complex structures, PhD dissertation, Swiss Federal Institute of Technology, Zurich, 2005, 193p.

[3] BREQUE, C., DUPRE, J.C., BREMAND, F., Calibration of a System of Projection-Moiré for Relief Measuring: Biomechanical Applications, Optics and Lasers in Engineering, 41: 241-260, 2004.

[4] SURREL, Y., Phase Stepping: a New Self-Calibrating Algorithm, Applied Optics, 32: 3598-3600, 1993.

[5] VIOTTI, M.R., KAUFMANN, G.H., Measurement of elastic moduli using spherical indentation and digital speckle pattern interferometry with automated data processing, Optics and Lasers in Engineering, 44: 495–508, 2006.

[6] Guide to the expression of uncertainty in measurement, Geneva: International Organisation for Standardization, 1993.

[7] KLINKOVA, O., DRAPIER, S., BERGHEAU, J.M., Simulation des contraintes résiduelles dans les structures composites: déformée après caisson et usinage, August 2009, Proceedings of the 19th French Congress of Mechanics, Marseille (France) O. DEBORDES, C. REY eds. Marseille: Electronic proceedings, 6 p. (in French).

[8] VIOTTI, M. R., KAUFMANN, G. H., Accuracy and sensitivity of a hole drilling and digital speckle pattern interferometry combined technique to measure residual stresses, Optics and Lasers in Engineering, 41: 297-305, 2004.